Electrocatalysis

How to cite:
International Edition: doi.org/10.1002/anie.202201604
German Edition: doi.org/10.1002/ange.202201604

Nitrate-to-Ammonia Conversion at an InSn-Enriched Liquid-Metal Electrode

*Jessica Crawford, Hanqing Yin, Aijun Du, and Anthony P. O'Mullane**

Abstract: The renewable energy driven electrochemical conversion of nitrates to ammonia is emerging as a viable route for the creation of this hydrogen carrier. However, the creation of highly efficient electrocatalysts that show prolonged stability is an ongoing challenge. Here we show that room temperature liquid metal Galinstan can be used as an efficient and stable electrocatalyst for nitrate conversion to ammonia achieving rates of up to 2335 $\mu g\,h^{-1}\,cm^{-2}$ with a Faradaic efficiency of 100 %. Density functional theory (DFT) calculations and experimental observation indicated the activity is due to InSn alloy enrichment within the liquid metal that occurs during the electrocatalytic reaction. This high selectivity for NH_3 is also due to additional suppression of the competing hydrogen evolution reaction at the identified In_3Sn active site. This work adds to the increasing applicability of liquid metals based on Ga for clean energy technologies.

The Haber–Bosch process used for industrial ammonia synthesis requires high temperatures (350–550 °C) and high pressures (150–250 atm),[1] making it energy intensive. 150 million tonnes of ammonia are produced annually, which accounts for approximately 1 % of global CO_2 emissions,[2] which in the US alone is predicted to increase at a rate of 2.3 % every year.[3] The process accounts for 3–5 % of the annual natural gas supply, totaling 1–2 % of the global energy supply.[4] For every tonne of ammonia produced, 1.5 tonnes of CO_2 is generated which contributes significantly to the greenhouse gas effect.[5] NH_3 is an extremely important chemical for food production as it is the main component in fertilisers,[6] however it has also been recognised as both a potentially sustainable liquid fuel and as an easy to handle hydrogen carrier. From an electrochemical viewpoint, there has been intense interest in the nitrogen reduction reaction (NRR) to produce NH_3, however the production rates are low due to the competing hydrogen evolution reaction and studies are often plagued by interference from impurities giving false results.[7]

A recent alternative is to electrochemically reduce NO_x species to produce NH_3.[8] In addition, NO_x species are a widespread pollutant in industrial wastewater, liquid nuclear waste, livestock excrement and chemical fertilisers. Therefore, using nitrates/nitrites to produce ammonia could in principle result in the production of a clean hydrogen carrier while simultaneously treating pollution sources. However, there are still significant issues that need to be addressed in terms of efficiency, stability and selectivity due to the various reaction pathways that are available as well as the competing HER. There have been some notable examples in this research area including single atom Fe catalysts,[9] copper-molecular solid catalysts[10] and CuPt foams,[11] however large scale production may be problematic for these types of materials. Therefore, there is an ongoing need to develop active catalysts that are simple to produce for large scale production of NH_3.

Liquid metals have recently emerged as promising materials that are highly active for both catalysis and electrocatalysis. For the former, liquid metal based materials have been employed for quite difficult reactions such as the catalytic reduction of CO_2 to solid carbon under both room temperature[12] and elevated temperature conditions[13] and the sonocatalytic reduction of organic dyes to solid carbon[14] indicating the excellent catalytic properties of these materials. Previous electrocatalytic studies have indicated that Ga based liquid metal composites can also electrochemically reduce CO_2 to solid carbon.[15] Therefore given these promising results there is significant potential for applying liquid metals to other electrocatalytic reactions, particularly given their stability.

Here, we use a Ga based liquid metal electrocatalyst for the electrochemical reduction of NO_x to NH_3 both for its catalytic potential but also because of its poor HER properties which should in principle increase the selectivity of the NO_x to NH_3 process. Specifically, we used Galinstan which is a eutectic alloy that is liquid at room temperature containing 68.5 % gallium, 21.5 % indium and 10 % tin as an electrocatalyst for converting NO_x species (NO_3^- and NO_2^-) to NH_3 in an acidic environment. The active sites generated within the liquid metal during the course of the reaction are

[*] J. Crawford, H. Yin, Prof. A. Du, Prof. A. P. O'Mullane
School of Chemistry and Physics,
Queensland University of Technology (QUT)
Brisbane, QLD 4001 (Australia)
and
Centre for Materials Science,
Queensland University of Technology (QUT)
Brisbane, QLD 4001 (Australia)
E-mail: anthony.omullane@qut.edu.au

experimentally determined which is supported by density functional theory (DFT) calculations.

Galinstan was coated onto copper substrates as a liquid layer ensuring the complete coverage of the substrate,[16] as shown in Figure S1. Cyclic voltammograms were then recorded in the absence and presence of nitrate species. Figure 1A shows a large increase in current over a potential range of −0.25 to −1.25 V vs. RHE when 100 mM HNO_3 is used compared to the control experiment containing 100 mM HCl. The cathodic current recorded in only 100 mM HCl (so that the same solution pH was used) shows a small peak at −0.9 V due to the reduction of oxides on the liquid metal surface while the further increase in current after this peak is due to the HER. This also illustrates one of the advantages of using a liquid Ga based system, i.e. the very large overpotential required to initiate the HER which offers a wide potential window to undertake other electrochemical reactions. Therefore, in 100 mM HNO_3 there is a large potential window where NO_3^- is reduced without any contribution to the current from the competing HER. The broad shoulder centred at −0.6 V is attributed to the reduction of NO_2^- produced during the initial stages of NO_3^- reduction. This is confirmed in Figure 1B which shows the reduction of NO_2^- at this catalyst in the region where there is no HER as indicated by the control experiment in acid in the absence of nitrite ions. Therefore, this data indicates that both NO_3^- and NO_2^- ions can be reduced at potentials where the HER does not occur. It should be noted that these cyclic voltammograms were initiated below the open circuit potential in each case to avoid liquid metal oxidation.

Chronoamperometry was then performed at applied potentials ranging from −0.34 to −1.04 V vs RHE for 1 hour to reduce NO_3^- to NH_3 (Figure 2A). The current density increases gradually going from −0.34 to −0.94 V, however it decreases at −1.04 V and becomes noisy indicating hydrogen bubble formation and some loss of contact of the electrode with the electrolyte. The Faradaic efficiency at each potential was then calculated (Figure 2B) and varies between 90–100 % over the potential range of −0.34 to −0.74 V where 100 % FE is achieved at the latter potential. This is followed by a gradual decrease in FE due to the competing HER. The NH_3 production rate was calculated for each applied potential for a 1 h duration and the highest rate was observed at −0.94 V giving a value of 2335 $\mu g_{NH_3}\, h^{-1}\, cm^{-2}$ which is one of the highest production rates reported so far for electrochemical reduction of nitrate to NH_3 (Table S1). The stability of the electrode was then tested under different conditions. Figure 2C shows a series of 1 h experiments undertaken at −0.74 V where the average rate calculated over the 10 experiments was determined to be 1166 $\mu g_{NH_3}\, h^{-1}\, cm^{-2}$ indicating its stability under start and stop conditions.

A continuous electrolysis experiment was also undertaken for 21 h at −0.94 V giving a production rate of 797 $\mu g_{NH_3}\, h^{-1}\, cm^{-2}$ (Figure S2) at 74 % FE over this time period which is promising as other reported electrocatalysts like Cu in a molecular solid reported a decrease in rate from 337.8 to 140.3 $\mu g\, h^{-1}\, cm^{-2}$ after 15 hours of electrolysis.[10] A digital image of the catalyst before and after electrolysis shows that the shiny metallic state is maintained (Figure S3).

To confirm that the electrochemical conversion of nitrate to ammonia is from the nitrate source that was used (HNO_3) rather than from contaminants or ambient ammonia, ^{15}N labelled $K^{15}NO_3$ was also used in H_2SO_4 to maintain the same pH. The production of NH_3 from both HNO_3 and ^{15}N labelled $K^{15}NO_3$ were confirmed using proton NMR (Figure 2D). The typical $^{14}NH_3$ triplet centred around 7 ppm when using $K^{14}NO_3$ was observed while the typical doublet was found when ^{15}N labelled $K^{15}NO_3$ was used.

Given that a trimetallic system is being used, the active site needs to be identified. Therefore, liquid Galinstan was

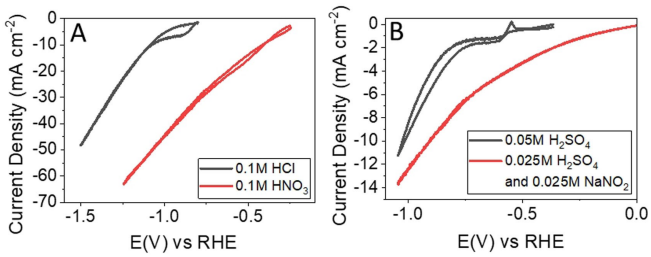

Figure 1. A) Cyclic voltammograms recorded at 20 $mV\, s^{-1}$ of a GaInSn film on a copper substrate in 0.1 M HCl and 0.1 M HNO_3 and B) in 0.05 M H_2SO_4 and a combination of 0.025 M H_2SO_4 and 0.025 M $NaNO_2$.

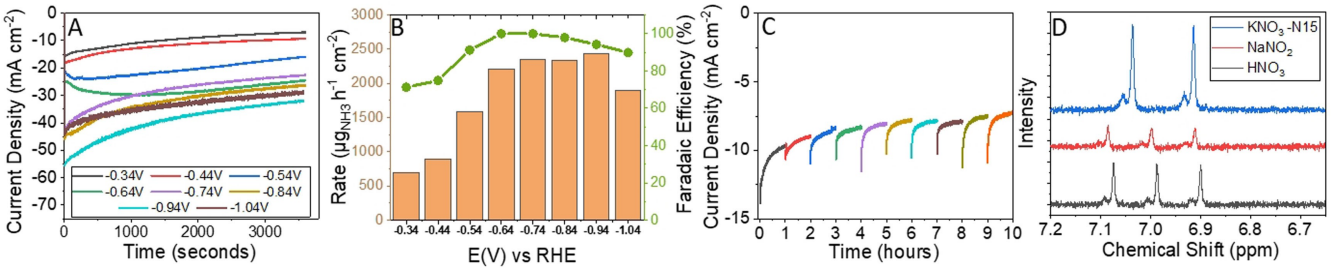

Figure 2. A) Shows the chronoamperometry performed at each potential for 1 hour with B) the resulting rates and faradaic efficiencies achieved using GaInSn film on a copper substrate. C) Stability of GaInSn on copper at −0.74 V vs. RHE for repetitive 1 h experiments and D) shows the NMR triplet associated with ammonia after nitrate reduction, nitrite reduction and the typical doublet after nitrate reduction using N-15 labelled KNO_3.

compared to the performance of liquid Ga. These experiments were conducted at 50 °C to ensure that Ga was in the liquid state and required a different setup as described in Supporting Information (Figure S4). It was found that Galinstan produced more NH_3 compared to Ga under identical conditions. This indicates that the In and Sn components are contributing significantly to nitrate/nitrite reduction and the presence of Ga can suppress the HER as indicated by the very high FE for the Galinstan electrode.

With this information a film of Galinstan was spread on a Cu electrode and imaged after nitrate reduction (Figure 3). Cu was chosen for the good wettability of GaInSn on Cu. From SEM imaging and EDX analysis (Figure 3) it was found that the morphology of the GaInSn film changes after 1 hour of nitrate reduction. For Galinstan an even distribution of Ga, In and Sn elements should occur[17] and the In:Sn ratio should be 2:1, however after nitrate reduction, not only does the morphology change, but the In:Sn ratio increases in many areas of the electrode indicating the formation of In–Sn rich regions within the predominantly Ga film. This is seen in the EDX mapping images showing the accumulation and co-location of In and Sn elements (Figure 3) while an EDX spectrum of one of these areas is shown in Figure S5 indicating a higher composition of In. It is known from literature that In_3Sn is a stable alloy of In and Sn which can be formed under mild conditions[18] and is likely contained in this InSn rich environment given that In_2Sn is not a preferred material.

This InSn enrichment process results from the formation of Ga_2Cu as it is known that Ga interacts with Cu as seen previously by Sarfo et al. who studied the interaction of liquid Galinstan with Cu collector electrodes under high applied currents where it was observed that gallium migrated into the copper layer leaving a surface layer rich in co-located In and Sn.[19] It should be noted that the Cu electrode was covered completely with the liquid metal and after electrolysis there was no evidence of Cu at the surface as indicated by X-ray photoelectron spectroscopy (XPS) (Figure 4). From the XPS spectra the presence of Ga, In and Sn was detected but not Cu. The Ga 2p spectrum showed peaks at binding energies of 1118.8 and 1145.6 eV corresponding to Ga $2p_{3/2}$ and Ga $2p_{1/2}$, respectively, indicating some oxidation of Ga. For the Sn 3d spectrum, peaks at binding energies of 485.2 eV (Sn $3d_{5/2}$) and 493.6 eV (Sn $3d_{3/2}$) are consistent with metallic tin. The In 3d spectrum showed peaks at 444.2 eV (In $3d_{5/2}$) and 451.7 eV (In $3d_{3/2}$), corresponding to metallic In with some surface oxidation present where peaks at 445.1 and 452.4 eV corresponding to In^{3+} were observed.[20] Therefore, any Ga_2Cu that was formed is beneath the surface layer of GaInSn and the enriched InSn regions. A further control experiment was undertaken using only a Ga film on a Cu substrate under identical electrolysis conditions (−0.74 V for 1 h) which resulted in a FE of 77 % compared to 100 % at the GaInSn electrode, indicating that Ga on Cu is active but much less so than GaInSn on Cu.

DFT calculations were then undertaken to understand if In_3Sn is the active component of the electrocatalyst (as it is a known stable form of In and Sn) and whether Ga_2Cu may also have some influence. The structural file of In_3Sn and Ga_2Cu was picked from the Materials Project Program.[21] To build a reasonable slab model, the surface energy of all low-index surfaces with different terminations was calculated (Table S2).[22,23] The In_3Sn(100-InSn) surface was selected because it has the second lowest surface energy and is terminated by both In and Sn. On these selected surfaces, the total nitrate reduction reaction ($NO_3^- + 9H^+ + 8e^- \rightarrow NH_3 + 3H_2O$) can be decomposed into deoxygenation and hydrogenation reactions in an acidic environment, according to previous reports,[24] and is outlined as follows:

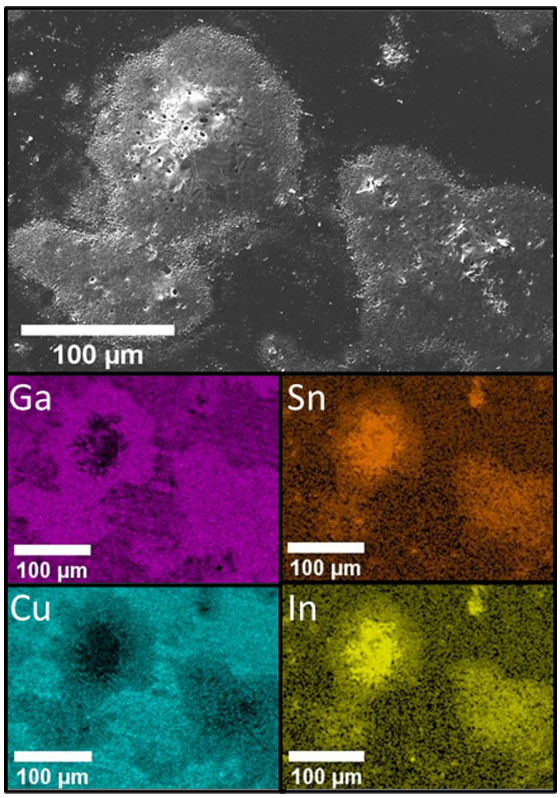

Figure 3. SEM image and EDX mapping of a GaInSn film on a Cu substrate after 100 mM nitrate reduction reaction for 1 hour at −0.74 V vs. RHE.

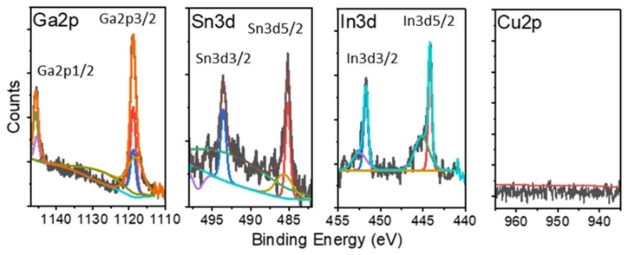

Figure 4. XPS spectra for Ga 2p, Sn 3d, In 3d and Cu 2p core levels for a GaInSn film on Cu substrate electrode after nitrate electrolysis at −0.74 V for 1 h.

$$NO_3^-(l) + * \rightarrow {}^*NO_3 + e^- \quad (1)$$

$${}^*NO_3 + 2H^+ + 2e^- \rightarrow {}^*NO_2 + H_2O \quad (2)$$

$${}^*NO_2 + 2H^+ + 2e^- \rightarrow {}^*NO + H_2O \quad (3)$$

$${}^*NO + 2H^+ + 2e^- \rightarrow {}^*N + H_2O \quad (4)$$

$${}^*N + H^+ + e^- \rightarrow {}^*NH \quad (5)$$

$${}^*NH + H^+ + e^- \rightarrow {}^*NH_2 \quad (6)$$

$${}^*NH_2 + H^+ + e^- \rightarrow {}^*NH_3 \quad (7)$$

$${}^*NH_3 \rightarrow * + NH_3(g) \quad (8)$$

All possible adsorption sites and configurations for each reaction intermediate (*NO_3, *NO_2, *NO, *N, *NH, *NH_2, *NH_3) were considered, and only those combinations possessing the lowest total free energy were used to clarify the reaction mechanism.[25] The most stable adsorption modes of each intermediate can be found in Figure 5. Based on the above mentioned mechanism and computational protocol, the free energy evolution for nitrate reduction was calculated (Figure 5) assuming the external potential as 0 V vs. RHE. Surprisingly, the free energy went completely downhill at each step along the proposed reaction pathway. This suggests that the catalytic performance is better on this catalyst than many other materials on which at least one energetically uphill step could be observed. Meanwhile the adsorption of nitrate has been reported to be a crucial step in the mechanism and could possibly be the Potential-Dependent Step (PDS) when ΔG_{ad} is positive.[25,26] Significantly, this was not found on our catalyst. It is also noteworthy that the desorption of NH_3 is almost spontaneous, thereby enhancing even further the excellent electrochemical performance of In_3Sn. On the other hand, nitrate reduction on Ga_2Cu-110 followed a similar trend till the last step where +0.27 eV is needed for ammonia desorption, suggesting the surface of Ga_2Cu might be blocked and further poisoned by strongly adsorbed NH_3 molecules (Figure S6). This comparison indicates that In_3Sn is the most active component of our catalyst for the NO_3RR. Another advantage of using liquid metals is that the surface does not easily foul as demonstrated by recent studies on electrochemical and sonochemical reduction of CO_2 to solid carbon[12,15] which does not stick to the surface due to the lack of van der Waals adhesion on the liquid surface which may aid with desorption processes.

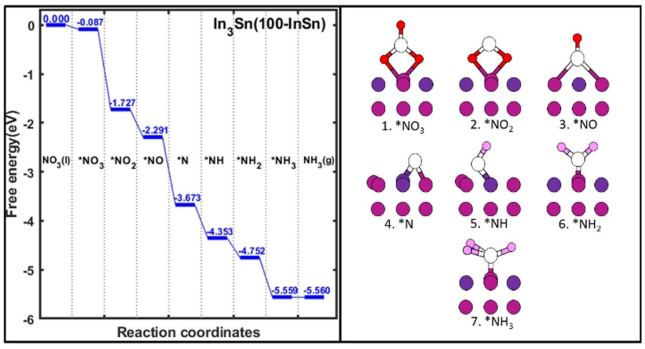

Figure 5. Free energy diagram of nitrate reduction on In_3Sn(100-InSn) and optimized structure of all intermediates. Grey: nitrogen; red: oxygen; mauve: tin; purple: indium; white: hydrogen.

In addition, DFT calculations were undertaken to evaluate the HER performance of the same surface of In_3Sn. There are multiple proton adsorption sites and therefore the binding energy (E_b) of all possible configurations were calculated (Table S3) because the free energy of proton adsorption is recognised as a descriptor of HER activity with an optimal value close to 0 eV.[27] The binding energies of all sites show large positive values (Figure S7), suggesting inhibition of the competing HER on In_3Sn which is consistent with the cyclic voltammetric data in Figure 1A. This inhibition of the HER may also be useful for other electrocatalytic reactions where selectivity is an issue due to this competing reaction.

In terms of cost, Ga and In are more expensive than Sn but are still considerably cheaper than precious metal electrocatalysts. However, with any emerging green energy technology the source of materials needs to be addressed. Ga is produced during bauxite processing,[28] which ultimately could be improved from a carbon footprint perspective via electrification of the process, while emerging Ga based technologies at end of life could in principle be recycled by electrochemical approaches to recover Ga.[29] Similarly there has been progress in recovering In and Sn from indium tin oxide sources via a sustainable chemical process with the generation of high purity In and Sn salts.[30] Indeed it was shown that Cu, In and Ga can be recovered electrochemically when CIGS solar cells are recycled.[29] Therefore the production of Ga, In and Sn can be viable from environmental and economic perspectives with appropriate measures.

In summary, a liquid metal Galinstan electrode immobilised on a Cu substrate shows excellent performance for the conversion of both nitrate and nitrite ions into ammonia at high rates with good selectivity and stability. The formation of enriched areas of InSn within the GaInSn film were confirmed by SEM/EDX analysis while DFT calculations indicated that In_3Sn is the active site for the reaction. This catalyst allows for the free energy of the reaction to go completely downhill along each step of the proposed reaction pathway while also inhibiting the often problematic HER.

Acknowledgements

The XPS and SEM data reported in this work were obtained at the Central Analytical Research Facility, QUT. AOM acknowledges support from the Australian Research Council (DP180102869). Open access publishing facilitated by Queensland University of Technology, as part of the Wiley - Queensland University of Technology agreement via the Council of Australian University Librarians.

Conflict of Interest

The authors declare no conflict of interest.

Data Availability Statement

The data that support the findings of this study are available from the corresponding author upon reasonable request.

Keywords: Ammonia Synthesis · Density Functional Calculations · Electrocatalysis · Liquid Metal · Nitrate Reduction

[1] a) J. Wang, L. Yu, L. Hu, G. Chen, H. Xin, X. Feng, *Nat. Commun.* **2018**, *9*, 1795; b) B. H. R. Suryanto, H.-L. Du, D. Wang, J. Chen, A. N. Simonov, D. R. MacFarlane, *Nat. Catal.* **2019**, *2*, 290.
[2] V. Kyriakou, I. Garagounis, A. Vourros, E. Vasileiou, M. Stoukides, *Joule* **2020**, *4*, 142.
[3] C. Smith, A. K. Hill, L. Torrente-Murciano, *Energy Environ. Sci.* **2020**, *13*, 331.
[4] Z. J. Schiffer, K. Manthiram, *Joule* **2017**, *1*, 10.
[5] Y. Bicer, I. Dincer, C. Zamfirescu, G. Vezina, F. Raso, *J. Cleaner Prod.* **2016**, *135*, 1379.
[6] J. M. Modak, *Resonance* **2002**, *7*, 69.
[7] X. Guo, J. Gu, S. Lin, S. Zhang, Z. Chen, S. Huang, *J. Am. Chem. Soc.* **2020**, *142*, 5709.
[8] a) R. Daiyan, T. Tran-Phu, P. Kumar, K. Iputera, Z. Tong, J. Leverett, M. H. A. Khan, A. Asghar Esmailpour, A. Jalili, M. Lim, A. Tricoli, R.-S. Liu, X. Lu, E. Lovell, R. Amal, *Energy Environ. Sci.* **2021**, *14*, 3588; b) X. Lu, H. Song, J. Cai, S. Lu, *Electrochem. Commun.* **2021**, *129*, 107094.
[9] Z.-Y. Wu, M. Karamad, X. Yong, Q. Huang, D. A. Cullen, P. Zhu, C. Xia, Q. Xiao, M. Shakouri, F.-Y. Chen, J. Y. Kim, Y. Xia, K. Heck, Y. Hu, M. S. Wong, Q. Li, I. Gates, S. Siahrostami, H. Wang, *Nat. Commun.* **2021**, *12*, 2870.
[10] G.-F. Chen, Y. Yuan, H. Jiang, S.-Y. Ren, L.-X. Ding, L. Ma, T. Wu, J. Lu, H. Wang, *Nat. Energy* **2020**, *5*, 605.
[11] G. A. Cerrón-Calle, A. S. Fajardo, C. M. Sánchez-Sánchez, S. Garcia-Segura, *Appl. Catal. B* **2022**, *302*, 120844.
[12] J. Tang, J. Tang, M. Mayyas, M. B. Ghasemian, J. Sun, M. A. Rahim, J. Yang, J. Han, D. J. Lawes, R. Jalili, T. Daeneke, M. G. Saborio, Z. Cao, C. A. Echeverria, F.-M. Allioux, A. Zavabeti, J. Hamilton, V. Mitchell, A. P. O'Mullane, R. B. Kaner, D. Esrafilzadeh, M. D. Dickey, K. Kalantar-Zadeh, *Adv. Mater.* **2022**, *34*, 2105789.
[13] K. Zuraiqi, A. Zavabeti, J. Clarke-Hannaford, B. J. Murdoch, K. Shah, M. J. S. Spencer, C. F. McConville, T. Daeneke, K. Chiang, *Energy Environ. Sci.* **2022**, *15*, 595–600.
[14] O. Oloye, J. D. Riches, A. P. O'Mullane, *Chem. Commun.* **2021**, *57*, 9296.
[15] D. Esrafilzadeh, A. Zavabeti, R. Jalili, P. Atkin, J. Choi, B. J. Carey, R. Brkljača, A. P. O'Mullane, M. D. Dickey, D. L. Officer, D. R. MacFarlane, T. Daeneke, K. Kalantar-Zadeh, *Nat. Commun.* **2019**, *10*, 865.
[16] S. N. S. Hapuarachchi, K. C. Wasalathilake, D. P. Siriwardena, J. Y. Nerkar, H. Chen, S. Zhang, Y. Liu, J.-c. Zheng, D. V. Golberg, A. P. O'Mullane, C. Yan, *ACS Appl. Energ. Mater.* **2020**, *3*, 5147.
[17] W. G. Kidanu, J. Hur, I. T. Kim, *Materials* **2022**, *15*, 168.
[18] Y. Zhao, Z. Zhang, H. Dang, *J. Mater. Chem.* **2004**, *14*, 299.
[19] D. K. Sarfo, R. R. Taylor, A. P. O'Mullane, *ACS Appl. Electron. Mater.* **2020**, *2*, 2921.
[20] M. Shafiei, F. Hoshyargar, N. Motta, A. P. O'Mullane, *Mater. Des.* **2017**, *122*, 288.
[21] A. Jain, S. P. Ong, G. Hautier, W. Chen, W. D. Richards, S. Dacek, S. Cholia, D. Gunter, D. Skinner, G. Ceder, *APL Mater.* **2013**, *1*, 011002.
[22] E. Heifets, R. Eglitis, E. Kotomin, J. Maier, G. Borstel, *Phys. Rev. B* **2001**, *64*, 235417.
[23] R. Eglitis, D. Vanderbilt, *Phys. Rev. B* **2007**, *76*, 155439.
[24] T. Hu, C. Wang, M. Wang, C. M. Li, C. Guo, *ACS Catal.* **2021**, *11*, 14417.
[25] Y. Wang, A. Xu, Z. Wang, L. Huang, J. Li, F. Li, J. Wicks, M. Luo, D.-H. Nam, C.-S. Tan, *J. Am. Chem. Soc.* **2020**, *142*, 5702.
[26] a) H. Liu, X. Lang, C. Zhu, J. Timoshenko, M. Rüscher, L. Bai, N. Guijarro, H. Yin, Y. Peng, J. Li, Z. Liu, W. Wang, B. R. Cuenya, J. Luo, *Angew. Chem. Int. Ed.* **2022**, *61*, e202202556; *Angew. Chem.* **2022**, *134*, e202202556; b) S. Zhang, M. Li, J. Li, Q. Song, X. Liu, *Proc. Natl. Acad. Sci. USA* **2022**, *119*, e2115504119; c) S. Guo, K. Heck, S. Kasiraju, H. Qian, Z. Zhao, L. C. Grabow, J. T. Miller, M. S. Wong, *ACS Catal.* **2018**, *8*, 503.
[27] J. K. Nørskov, T. Bligaard, A. Logadottir, J. Kitchin, J. G. Chen, S. Pandelov, U. Stimming, *J. Electrochem. Soc.* **2005**, *152*, J23.
[28] M. Frenzel, M. P. Ketris, T. Seifert, J. Gutzmer, *Resour. Policy* **2016**, *47*, 38.
[29] A. M. K. Gustafsson, F. Björefors, B.-M. Steenari, C. Ekberg, *Sci. World J.* **2015**, *2015*, 494015.
[30] S. Gu, B. Fu, G. Dodbiba, T. Fujita, B. Fang, *RSC Adv.* **2017**, *7*, 52017.

Manuscript received: January 28, 2022
Accepted manuscript online: March 23, 2022
Version of record online: ■■, ■■

Communications

Electrocatalysis

J. Crawford, H. Yin, A. Du,
A. P. O'Mullane* _____ e202201604

Nitrate-to-Ammonia Conversion at an InSn-Enriched Liquid-Metal Electrode

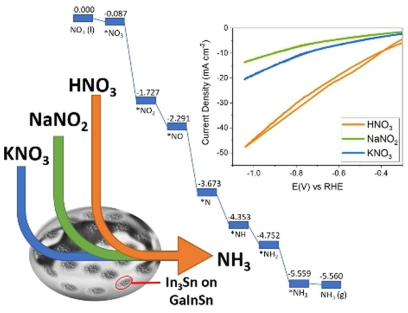

In this work a Ga-based liquid metal electrocatalyst is developed for the electrochemical conversion of nitrate and nitrite ions to ammonia at room temperature where InSn is identified as the active site for the reaction.